I-V curve of the electron flow generated during a pyroelectric effect in lithium tantalate single crystal in vacuum conditions

A.N. Oleinik[1, *], M.E. Gilts[1], P.V. Karataev[2], A.A. Klenin[1], A.S. Kubankin[1,3], P.G. Shapovalov[4]

[1] *Laboratory of Radiation Physics, Belgorod, Russia*
[2] *John Adams Institute at Royal Holloway, University of London, Egham, TW20 0EX, United Kingdom*
[3] *Lebedev Physical Institute, Moscow, Russia*
[4] *National Research Nuclear University "MEPhI", Moscow, Russia*
* oleynik_a@bsu.edu.ru

Annotation

Realization of pyroelectric effect in vacuum provides a possibility to develop a compact and relatively inexpensive electron source. In this article we observed and analyzed the I-V curve of electron flow generated during the pyroelectric effect in lithium tantalate single crystal. The region of the monoenergetic electron flow with a slow change in the peak energy is determined. This phenomenon is accompanied by a current avalanche process. Analysis of the electron spectra and the I-V curve shows that the observed avalanche process and the stabilization of the peak energy occurs due to a sharp increase of secondary electrons in the total electron flow.

1. Introduction

Electrification of dielectrics in vacuum can be used to generate a high electric field of up to 10^6 V/cm [1]. The electrification of materials with spontaneous polarization is an area of particular interest, because the electric field can be generated by external mechanical or thermal influence known as the piezoelectric or the pyroelectric effect respectively [1,2]. The high electric field leads to a so-called field electron emission either from the charged surface or from the surrounding conductors depending on the sign of the induced charge [3]. This phenomenon underlies the pyroelectric and piezoelectric accelerator concepts. In these devices, electrons are accelerated to the energy of the order of several tens of keVs [4,5]. Such type of accelerator can be used to generate X-rays, neutrons, positive ions, as well as to control charged particle beams. On the other hand, it is considered as a cheap and simple instrument for operation under non-standard conditions [6-13].

The emitted electrons have two remarkable properties: the flow is self-focused at a certain distance from the emission plane [12] and is monoenergetic with slowly changing value of energy. The latter phenomenon is not fully understood. Simultaneous measurement of current and voltage makes it possible to obtain the V-I dependence, which is widely used to describe the properties of devices and structures under test [14,15]. However, it is very difficult to measure the potential difference between the pyroelectric material and the target directly. We found two indirect ways to evaluate the potential. The first way is to determine the endpoint energy of the X-ray spectrum, which cannot be higher than the potential difference [16]. However, the accuracy of this method depends on the position of the X-ray detector and the X-ray flux intensity. The second way is a direct measurement of the electron flux, where the peak is observed and its position defines the potential difference [1,4].

Both ways are implemented in this work to determine the I-V curve of the electron flow during the pyroelectric excitation of lithium tantalate single crystal ($LiTaO_3$, LT), which has a large pyroelectric coefficient comparing to other pyroelectric materials [17]. The periodic temperature variation is used to change the temperature of the crystal [18]. Standard geometry of

the pyroelectric accelerator [10-13] is modified to measure the current and the electron spectrum simultaneously. Based on the analysis of the I-V curve and electron spectra, we can distinguish the primary electron flux of electrons emitted from the surface of the LT sample and the secondary electron flux, produced predominantly from the metallic target being irradiated. The avalanche process is associated with a sharp increase of the number of the secondary electrons and leads to the primary electron flux stabilization. However, the flux peak becomes less intense and broader during the avalanche process, which may indicate a distortion of the emitted electron flow.

2. Experiment

The geometry of the pyroelectric accelerator is shown in Figure 1a. The target was a brass place of 400 μm thick with a 0.3 mm hole. The target is mounted coaxially with the vertical axis passing through the center of the polar surface of LT single crystal (*2*). The crystal has a cylindrical shape (Z-axis is co-directed with the cylinder guide) with diameter of 20 mm and the height of 10 mm. The area of the target is much larger than the polar LT crystal surface. An aluminum foil (*3*), which served as the second electrode in the electric circuit was attached to the crystal with a conductive epoxy glue. The Peltier element *(4)* is used to apply the temperature changing in time. The reverse side of the Peltier element is glued to an aluminum heatsink (*5*) for efficient heat exchange. The electron detector Ortec CR-012-025-100 (*6)* was located 30 mm behind the target coaxially with the hole. The X-ray spectrometer Amptek Cd-Te X-123 (*7*) mounted through a side flange was used to measure X-ray emission from both the crystal and the target surfaces.

The target served as an electrode for closing the current measurement circuit. A part of the electrons passed through the hole and registered by the detector. The measurement of the electron current was carried out by connecting the target and the foil glued to the lower surface of the LT crystal into a circuit through the picoammeter Keithley 6485 [13]. The temperature of the pyroelectric material was changed in a sinusoidal mode [18] with the frequency of 0.5 mHz and the amplitude of 18°C near the top crystal surface (the temperature changed between 20 °C and 38 °C). The typical vacuum level was varied from 0.05 to 50 mTorr. The vacuum level was controlled using the manual valve. The change is happened in the pause between the half-waves of the generated particles, i.e., in the maximal or minimal temperature. During active particle generation, the pressure was almost constant. The vacuum control was provided by a forevacuum (Geowell GWSP150) and a turbomolecular (Oerlikon TMP50) pumps. Here we present results only during the negative polarity phase, when the negative charge induced on the upper polar surface and emission occurs from the crystal.

3. Results and discussion

Figures 1(b) and 1(c) present the evolution of the electron and X-ray spectra during a half-cycle of temperature variation at the negative polarity phase. The energy of the electron peak increases, but, at the same time, the peak amplitude decreases and the width increases. A sharp increase in the continuous background along with an increase in the peak energy is associated with growth of the secondary electron production. The X-ray spectrum contains the characteristic lines of copper and zinc from the brass target, iron and chromium lines from the vacuum chamber wall. The endpoint energy of the X-ray spectrum increases following the electron peak energy up to 35 keV. However, after that the endpoint energy saturates while the peak energy keeps on growing until it, becomes noticeably higher. A small number of high-energy photons can be associated with a non-optimal position of the X-ray detector, when radiation emission from the target is observed at the acute angle of 3°. This is a demonstration that the electron peak energy monitoring is a more accurate way to determine the potential difference.

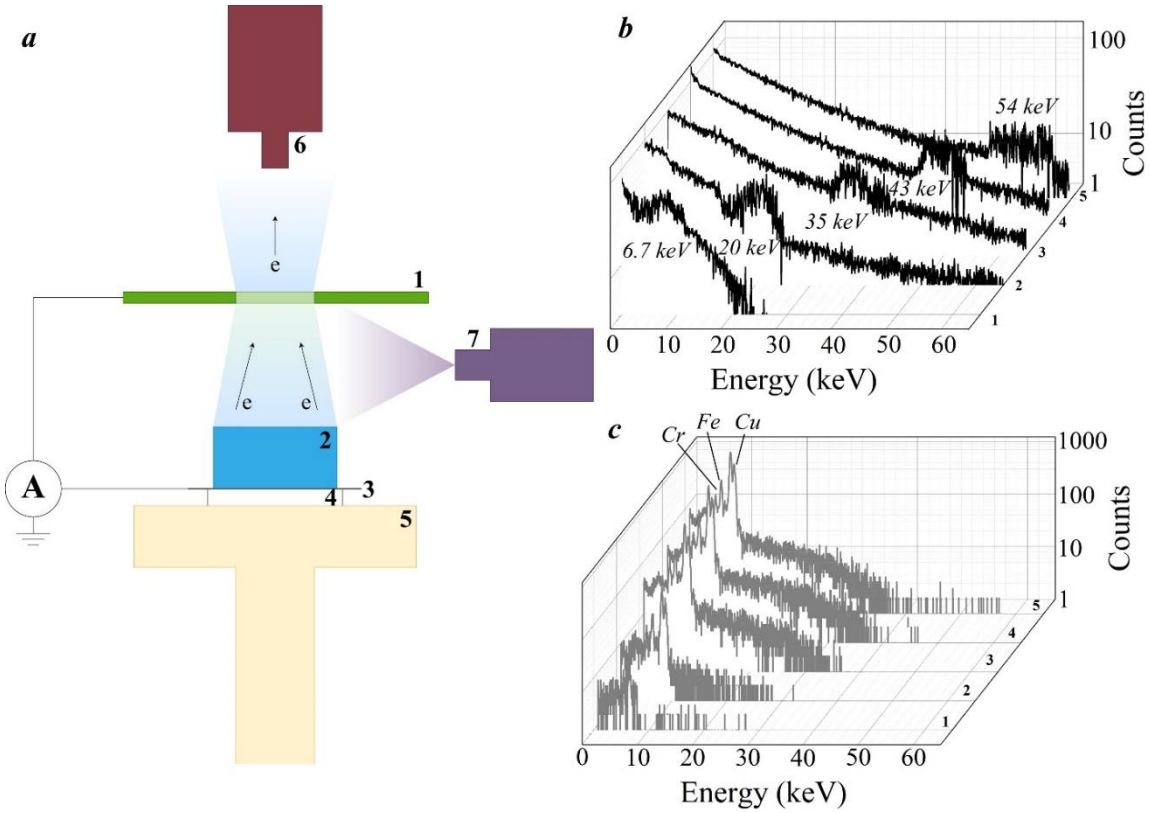

Figure 1. (a) Scheme of experiment. 1 – Brass target, 2 –$LiTaO_3$ single crystal, 3 – Aluminum foil, 4 – Peltier element, 5 – Aluminum heat sink, 6 – Electron detector, 7 – X-ray detector. Evolution of the electron (b) and X-ray (c) spectra during a half-cycle of temperature variation at the negative polarity phase. Numbers at Figures 1b and 1c correspond to numbers at Figure 2.

The electron and X-ray fluxes versus time during a half-cycle of temperature variation and at residual gas pressure of 1 mTorr are shown in Figure 2. A sinusoidal electron current with the amplitude of about 115 pA is observed. An additional wave is superimposed on the second half of the sine function, so that the total current level reaches 400 pA. The additional and main wave go down together until the current polarity reverses, i.e. the transition to the positive polarity, when the electrons move from the target to the LT crystal. The maximal number of electron counts in the spectrum is observed a bit later than the maximum of the current curve. The peak of monoenergetic electrons in the spectrum appears closer to the maximum of the main current wave and disappears along with the change of polarity. The peak energy is stable during the additional current wave only. The numbers indicate the points corresponding to the spectra in Figure 1. Spectra 4 and 5 were taken during the additional electron wave with slight difference in the peak position, which also indicates the stabilization of the particle generation process.

The I-V curve of the electron flux, based on the peak energy and electron current measurement (see Fig. 2) is shown in Figure 3a. The additional wave forms a closed hysteresis loop with the peak energy changing by no more than 20% within 350 seconds. The observed I-V curve is very similar to the non-self-sustained Townsend discharge [19-21]. It allows us to assume that the observed additional wave is an avalanche process, and the stabilization of the peak energy is associated with this discharge. The I-V curve depends on the residual gas pressure as shown in Figure 3b. The higher pressure increases the probability of impact ionization of residual gas molecules, which is the main mechanism for initiation of the Townsend discharge [19]. However, in our case, an increase in pressure leads to a distortion of the I-V curve and the weakening of the discharge. Therefore, the observed avalanche process is not the Townsend discharge.

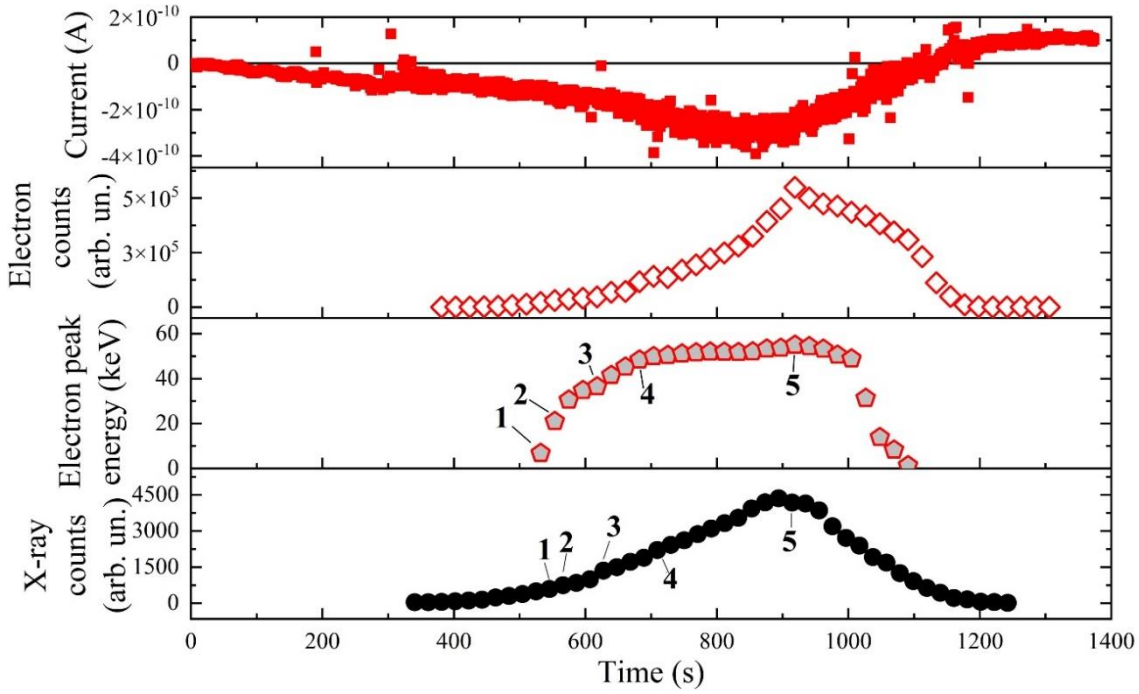

Figure 2. The parameters of electron and X-ray fluxes during a half-cycle of temperature variation at a residual gas pressure of 1 mTorr. From top to bottom: electron current, number of counts in electron spectra, energy of electron peak, number of counts in X-ray spectra. The numbers correspond the numbers at Figure 1.

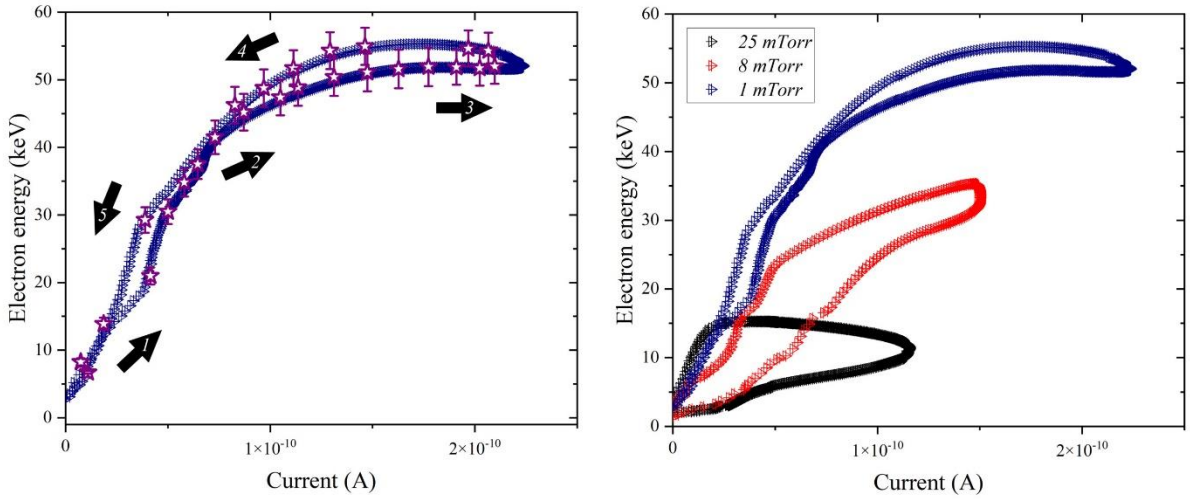

Figure 3. (a) The I-V curve of the electron flux based on data from Fig. 2. (b) - I-V curve of the electron flux at different values of residual gas pressure. The course of the curve is shown by numbered arrows. For the curves in Fig. 3b it is similar.

The main contribution to the background of the electron spectrum comes from secondary electrons, including those that are kicked out of the target. The spectra presented in Figure 1, demonstrate a sharp increase in the secondary electron contribution. Previously, it was shown that one of the indicators of the stability of the pyroelectric accelerator is the peak/total ratio (the number of events in the peak to the total number of events in the spectrum [22]). Figure 4 presents the change of the peak/total ratio for all three I-V curves presented in Figure 3. First, that the peak/total ratio first slowly increases during the sharp increase of the current (the start of the avalanche), and then drops down when the current reaches the maximum (the maximum of the

avalanche). It should be noted that the growth of the peak/total ratio is much slower than the growth of the total number of events in the electron spectrum. Therefore, during the avalanche discharge and stabilization of the peak energy, the current growth occurs due to impact ionization of the target material. Thus, we can assume that the avalanche discharge and the stabilization of the peak energy (and hence the stabilization of the potential difference) are observed due to the influence of secondary electron emission from the target.

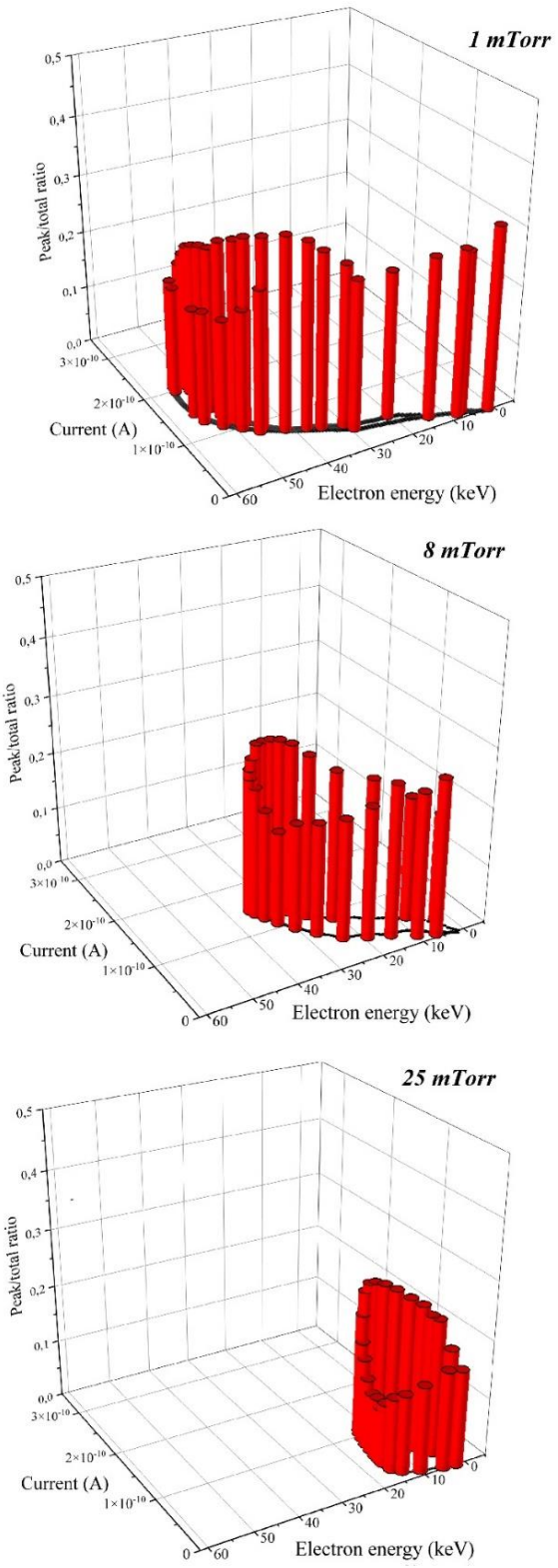

Figure 4. The peak/total ratio for I-V curves from Fig 3.

An increase in pressure leads to a gradual suppression of the flow of secondary electrons [23] and reduction of the amplitude of the avalanche process. In turn, the energy of the monoenergetic electrons also decreases. As a result, the electron energy peak smears out and gradually disappear. The above effects cause the median value of the peak/total ratio to drop. Thus, the monoenergetic electron flow with a slow change in the energy might appear due to the secondary electrons, which cannot leave the region between the crystal and the target. These electrons take out a part of the power induced by the temperature change preventing further accumulation of the potential.

4. Conclusion

Simultaneous measurement of the current and the electron spectrum in pyroelectric accelerator allows to obtain the I-V curve. A remarkable detail of the I-V curve is a hysteresis loop with energy of the electron peak changing slowly. An additional wave is observed in the current providing evidence of the avalanche process. The shape of the curve is similar to the I-V curve of a non-self-sustaining Townsend discharge, however, the conditions for the avalanche initiation are principally different. The avalanche weakens when pressure level increases. The peak/total ratio [22] drops during the avalanche indicating that the main source of additional electrons is the target, but not the residual gas. An important fact is the observation of peak energy stabilization during the avalanche demonstrating their relationship. However, the peak itself becomes weaker and wider indicating that the monoenergetic electron flow is distorted.

The study of the avalanche process, the conditions for its occurrence and the possibilities of maintaining the primary electron flow with stable energy have become new goals in the study of the electron generation in the pyroelectric accelerator. The key influence of the secondary electron emission suggests that the target material with different secondary electron emission coefficient needs to be investigated. From a practical point of view, the correct selection of the target material provides a possibility to regulate the long-term monoenergetic phase of the electron flow, which, of course, is a driver for the development of practical devices based on the concept of the pyroelectric accelerator.

Acknowledgement

The research was supported by a grant from the Russian Science Foundation (Project No. 21–72–00006). The work of A.K. (creation of the experimental setup) was financially supported by a Program of the Ministry of Education and Science of the Russian Federation for higher education establishments, Project No. FZWG-2020-0032 (2019-1569). The work of P.K. (conceptualization, supervision, manuscript preparation) was supported by the Science and Technology Facilities Council via John Adams Institute for Accelerator Science at Royal Holloway, University of London (Grant Ref. No. ST/V001620/1).

References

[1]. Brownridge J.D., *Electron and positive ion beams and x-rays produced by heated and cooled pyroelectric crystals such as $LiNbO_3$ and $LiTaO_3$ in dilute gases: phenomenology and applications*, Trends in Electro-Optics Research, (Nova Science Publishers, New-York) 2005, pp. 57-74 ISBN:978-1594544989

[2]. Tagantsev A., Pyroelectric, piezoelectric, flexoelectric, and thermal polarization effects in ionic crystals, *Sov. Phys. Usp.* **30** (1987) 588–603. DOI: 10.1070/PU1987v030n07ABEH002926

[3]. Rosenman G. et. al., Electron emission from ferroelectrics, J. Appl. Phys. **88** (2000) 6109. DOI:10.1063/1.1319378

[4]. Geuther J.A., Danon Y., Electron and positive ion acceleration with pyroelectric crystals, *J. Appl. Phys.* **97** (2005) 074109. DOI: 10.1063/1.1884252
[5]. Ivashchuk O.O. et al., Piezoelectric accelerator, *Sci. Rep.* **8** (2018) 16488. DOI: 10.1038/s41598-018-34831-8
[6]. Geuther J.A., Danon Y., High-energy x-ray production with pyroelectric crystals, *J. Appl. Phys.* **97** (2005) 10491. DOI: 10.1063/1.1915536
[7]. Naranjo B., Gimzewski J., Putterman S., Observation of nuclear fusion driven by a pyroelectric crystal, *Nature* **434** (2005) 1115. DOI: 10.1038/nature03575
[8]. Geuther J.A., Danon Y., Saglime F., Nuclear reactions induced by a pyroelectric accelerator, *Phys. Rev. Lett.* **96** (2006) 54803. DOI: 10.1103/PhysRevLett.96.054803
[9]. Oleinik A.N. et. al., Pyroelectric deflector of charged particle beam, *JINST* **11** (2016) P08007. DOI: 10.1088/1748-0221/11/08/P08007
[10]. Wilke M. et. al., Focusing of x-rays emitted by a pyroelectric x-ray generator for micro x-ray fluorescence, *J. of Vac. Sci. Tech. B* **37** (2019) 011203. DOI: 10.1116/1.5067322
[11]. Ghaderi R., Davani F.A., Dynamics of pyroelectric accelerators, *Appl. Phys. Lett.* **106**, (2015) 042906. DOI: 10.1063/1.4906866
[12]. Brownridge J.D., Shafroth S.M., Self-Focused Electron Beams Produced by Pyroelectric Crystals on Heating or Cooling in Dilute Gases, *Appl. Phys. Lett.* **79** (2001) 3364. DOI:10.1063/1.1418458
[13]. Brownridge J.D. et. al., Observation of multiple nearly monoenergetic electron production by heated pyroelectric crystals in ambient gas, *Appl. Phys. Lett.* **78** (2001) 1158. DOI:10.1063/1.1342209
[14]. Huo W., Zhou H., Du C., Effect of doping concentration of tunnel junction on I-V characteristics of photovoltaic power converter, *Europhys. Lett.*, **139** (2022) 56002. DOI: 10.1209/0295-5075/ac8ac8
[15]. Joachim C., Gimzewski J. K, Effect of doping concentration of tunnel junction on I-V characteristics of photovoltaic power converter, *Europhys. Lett.*, **30** (1995) 409. DOI: 10.1209/0295-5075/30/7/006
[16]. Oleinik A.N. et. al., Dependence of the Endpoint Energy of X-Ray Radiation on the Preliminary Temperature Change during the Pyroelectric Source Operation in the Pulsed Mode, *Bull. Lebedev Phys. Inst.* **48** (2021) 127. DOI:10.3103/S1068335621050079
[17]. Geuther J.A., Radiation generation with pyroelectric crystals, Ph.D. Thesis, Rensselaer Polytechnic Institute (2007). URL: https://hdl.handle.net/20.500.13015/3836
[18]. Oleinik A.N. et. al., Peculiarities of the pyroelectric current generated using a LiNbO3 single crystal driven by low-frequency sinusoidal temperature variation, *J. Appl. Phys.* **132** (2022) 204101. DOI: 10.1063/5.0124599
[19]. Massines F., et. al., Glow and Townsend dielectric barrier discharge in various atmosphere, *Plasm. Phys. Control. Fusion* **47** (2005) B577. DOI:10.1088/0741-3335/47/12B/S42
[20]. Xiao D., Fundamental Theory of Townsend Discharge, Springer, 2016. ISBN:978-3-662-48041-0
[21]. Luo H., Wang X., Li C., Extraordinary extinction of dielectric barrier Townsend discharge in nitrogen at atmospheric pressure, *Europhys. Lett.*, **97** (2012) 15002. DOI 10.1209/0295-5075/97/15002
[22]. Karataev P. et. al., Indicators of upcoming electric breakdown in a pyroelectric accelerator, *App. Phys. Exp.* **15** (2022) 066001. DOI: 10.35848/1882-0786/ac6b82
[23]. Arumugam S., et. al., Effective Secondary Electron Emission Coefficient of Brass, *Current Smart Materials* **2** (2017) 44. DOI: 10.2174/2405465801666160824144452